

Spin polarization of graphene and *h*-BN on Co(0001) and Ni(111) observed by spin-polarized surface positronium spectroscopy

A. Miyashita, M. Maekawa, K. Wada, A. Kawasuso,* T. Watanabe, S. Entani, and S. Sakai
National Institutes for Quantum and Radiological Science and Technology, 1233 Watanuki, Takasaki, Gunma 370-1292, Japan



(Received 1 February 2018; revised manuscript received 24 April 2018; published 4 May 2018)

In spin-polarized surface positronium annihilation measurements, the spin polarizations of graphene and *h*-BN on Co(0001) were higher than those on Ni(111), while no significant differences were seen between graphene and *h*-BN on the same metal. The obtained spin polarizations agreed with those expected from first-principles calculations considering the positron wave function and the electron density of states from the first surface layer to the vacuum region. The higher spin polarizations of graphene and *h*-BN on Co(0001) as compared to Ni(111) simply reflect the spin polarizations of these metals. The comparable spin polarizations of graphene and *h*-BN on the same metal are attributed to the creation of similar electronic states due to the strong influence of the metals: the Dirac cone of graphene and the band gap of *h*-BN disappear as a consequence of *d*- π hybridization.

DOI: [10.1103/PhysRevB.97.195405](https://doi.org/10.1103/PhysRevB.97.195405)

I. INTRODUCTION

Graphene is a semimetal with an extremely high carrier mobility and a long spin relaxation time. Hence graphene is expected to be a good spin conductor [1]. An ordinary way to inject excess spins into graphene is to place it in contact with a ferromagnet. The induced spin polarization is called the proximity effect. Its physical origin is the modulation of the electronic state of graphene due to hybridization with the ferromagnet. An alternative method is tunneling injection through barrier materials. Since single layer hexagonal boron nitride (*h*-BN) is an insulator with a band gap of 5–6 eV, inserting it between the ferromagnet and the graphene may make tunneling spin injection feasible [2].

Previous work based on spin-polarized metastable-atom deexcitation spectroscopy (SPMDS) has shown the appearance of a new electronic state in graphene on Ni(111) that exhibits spin-polarized metallic conduction [3]. The ferromagnetism of graphene decorated with Co atoms is explained in terms of charge transfer from the Co atoms to the graphene [4]. Co-intercalated graphene shows an out-of-plane spin polarization [5]. SPMDS studies have shown that *h*-BN on Ni(111) also exhibits spin-polarized metallic conduction arising from the in-gap states [6]. A theoretical study has suggested that *h*-BN on Co(0001) may be metallic, while *h*-BN on Ni(111) is half-metallic [7]. If this is correct, then *h*-BN attached to metals would hardly maintain its insulating properties, which would inhibit tunneling spin injection. It is, therefore, important to investigate the spin polarization of graphene and *h*-BN on Co(0001) and Ni(111) more systematically.

In this research, we employed spin-polarized surface positronium annihilation spectroscopy. This method is assured to detect the electron spin polarization of the first surface layer [8–11]. The results show that, in both graphene and *h*-BN on both Co(0001) and Ni(111), electrons have a

similar positive spin polarization. First-principles calculations explain that this similarity between graphene and *h*-BN is due to the appearance of similar electronic structures in graphene and *h*-BN when they are attached to Co(0001) and Ni(111).

II. EXPERIMENT

In the sample preparation, first, 30 nm thick films of Co(0001) and Ni(111) were grown on Al₂O₃(0001) using an electron beam evaporator. Subsequently, graphene and *h*-BN layers were grown on the metal films by ultrahigh vacuum chemical vapor deposition (CVD) [6,12,13]. As references, graphene and *h*-BN layers on paramagnetic Ru(0001) were also prepared in a similar manner. After the growth of graphene and *h*-BN, the flatness, morphology, and chemical composition were checked using reflection high-energy electron diffraction, scanning tunneling microscopy, and photoelectron spectroscopy, respectively. The samples were transferred through air to a vacuum chamber (base pressure: 1×10^{-7} Pa) equipped with a positron beam apparatus. The samples were cleaned by heating at 1000 K for 30 min. In this treatment, most of the adsorbates, mainly carbon hydrides and oxides, were removed.

Figure 1(a) shows the schematics of the measurement system. Transversely spin-polarized positrons with an energy of 200 eV were injected into the sample. Some of these positrons return to the surface and are emitted into the vacuum as positronium (an electron-positron bound state) by picking up surface electrons. Spin-singlet ($S = 0$) positronium annihilates into two photons, while spin-triplet ($S = 1$) positronium annihilates into three photons. Two-photon events create a sharp peak at 511 keV ($=m_0c^2$, where m_0 is the electron rest mass and c is the speed of light). Three-photon events give rise to a continuous spectrum below 511 keV. Figure 1(b) shows the typical annihilation photon energy spectra for 0% (mica at room temperature) and 100% (Ge at 1000 K) positronium formation. The spectrum intensities are normalized to the 511 keV peak. Denoting the intensities of the shaded

*Corresponding author: kawasuso.atsuo@qst.go.jp

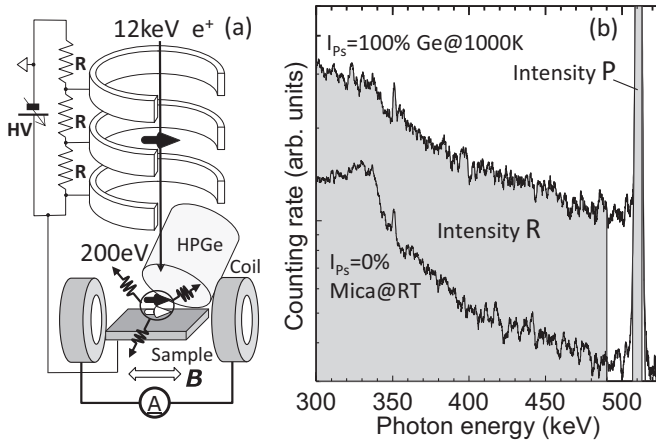


FIG. 1. (a) Schematic diagram of the experimental setup. A positron beam with an energy of 12 keV is decelerated to 200 eV and injected into the sample. Some of the positrons reach the sample surface and are emitted as positronium into the vacuum. Annihilation photons are observed by a Ge detector. The positron beam is transversely spin polarized with $P_+ = 0.3$. The sample is in-plane magnetized by a Helmholtz coil with a field strength of 30 mT. (b) Energy spectra of annihilation photons for 0% (mica at room temperature) and 100% (Ge at 1000 K) positronium formation. The intensities are normalized to the 511 keV peak intensity. The shaded areas define the intensities R and P in Eq. (1).

areas in Fig. 1(b) as R and P , the positronium intensity is given by

$$I_{P_s} = \left[1 + \frac{P_{100\%}}{P_{0\%}} \frac{R_{100\%} - R}{R - R_{0\%}} \right]^{-1}, \quad (1)$$

where the subscript of 100% or 0% denotes positronium intensity [14–16]. Though I_{P_s} is between zero and 1, the actual positronium three-photon intensity is given, for instance, by multiplying by 3/4 for a spin-compensated system. The three-photon intensity is higher (lower) when positron and electron spins are parallel (antiparallel). Based on this, measuring the field-reversal asymmetry of positronium intensity gives the surface spin polarization (P_-) as

$$P_- = \frac{1}{\alpha P_+} \frac{I_{P_s}(-M) - I_{P_s}(+M)}{I_{P_s}(-M) + I_{P_s}(+M)}, \quad (2)$$

where P_+ ($=0.3$) is the positron spin polarization, α ($=0.6$) is the coefficient determined from the spin-dependent detection efficiency of annihilation photons [17], and $\pm M$ indicates whether the magnetization direction is parallel (+) or antiparallel (–) to the positron spin polarization. From Eq. (2), positive (negative) P_- indicates that the number of majority (minority) spin electrons is more than that of minority (majority) spin electrons.

The ferromagnetic layers were in-plane magnetized by a magnetic field of 30 mT. All the measurements were conducted in remanence. To avoid any artificial effects of the magnetic field, the direction of the magnetic field was always fixed (in the positive or negative direction) and the magnetization direction with respect to the positron spin polarization direction was changed by rotating the sample. The sample holder was made of only nonferromagnetic materials. In each experiment,

eight spectra were acquired: four spectra were recorded for the positive direction and four for the negative direction. In each spectrum, total counts of 4×10^5 were accumulated. Subsequently, the electron spin polarization was obtained using Eq. (2). For each sample, the above protocol was repeated more than four times. The final spin polarization was determined by averaging these measurements.

III. THEORETICAL CALCULATION

To interpret the experimental data quantitatively, density functional theory (DFT) calculations were carried out using ABINIT code [18] with the projector-augmented-wave method [19] within the generalized gradient approximation (GGA) [20]. The initial valence electron configurations were assumed to be $3s^2 3p^6 3d^7 4s^2$ (Co), $3s^2 3p^6 3d^8 4s^2$ (Ni), $2s^2 2p^2$ (C), $2s^2 2p^1$ (B), and $2s^2 2p^3$ (N). The Co(0001) and Ni(111) films were composed of 7 monolayers stacked in the surface normal direction and the primitive cell was aligned parallel to the surface. For graphene, C atoms were distributed to on-top and fcc positions of the Co(0001) and Ni(111) surfaces. For h -BN, B and N atoms were distributed to fcc and on-top positions, respectively, of the Co(0001) and Ni(111) surfaces. The back surfaces were treated in the same way to avoid any artificial effects arising from asymmetry. The van der Waals potential was also considered [21]. The vacuum layer was initially assumed to be 20 Å. For the electron calculation, the number of k points sampled was $9 \times 9 \times 1$. For the positron calculation only the Γ point was considered. Full structural optimization was carried out in all the calculations.

IV. RESULTS AND DISCUSSION

A. Experiment

In all samples, the positronium intensity was found to increase from $\sim 30\%$ before heat treatment to more than 60% after heat treatment. Also, no spin polarizations were observed without heat treatment. Figure 2 shows the spin polarizations obtained for all the samples. Here, Eq. (2) is rewritten as $P_- = \Delta P_- (+M) - \Delta P_- (-M)$ and the values of $\Delta P_- (\pm M) = \frac{1}{\alpha P_+} \frac{I_{P_s}(\pm M) - [I_{P_s}(-M) + I_{P_s}(+M)]/2}{I_{P_s}(-M) + I_{P_s}(+M)}$ are plotted in the figure. The average spin polarizations are shown below each panel. After heat treatment, finite spin polarizations appear for graphene and h -BN on Co(0001) (+3–+4%) and Ni(111) (+1–+2%). No spin polarization is seen for either graphene or h -BN on paramagnetic Ru(0001). Thus the spin polarization is induced from Co and Ni to graphene and h -BN after heat treatment, even though the samples have been once exposed to air. In addition, the induced spin polarizations were persistently observed after heat treatment for at least 4 days. This means that Co and Ni surfaces covered by graphene and h -BN are quite inert.

Figure 3 shows the temperature dependence of spin polarization for graphene and h -BN on Co(0001) and Ni(111). Spin polarizations for graphene and h -BN on Co(0001) are unchanged up to 700 K, while those for graphene and h -BN on Ni(111) disappear at 700 K. Thus the spin polarizations of graphene and h -BN are lost above the Curie temperature for the ferro- to para-magnetic transition.

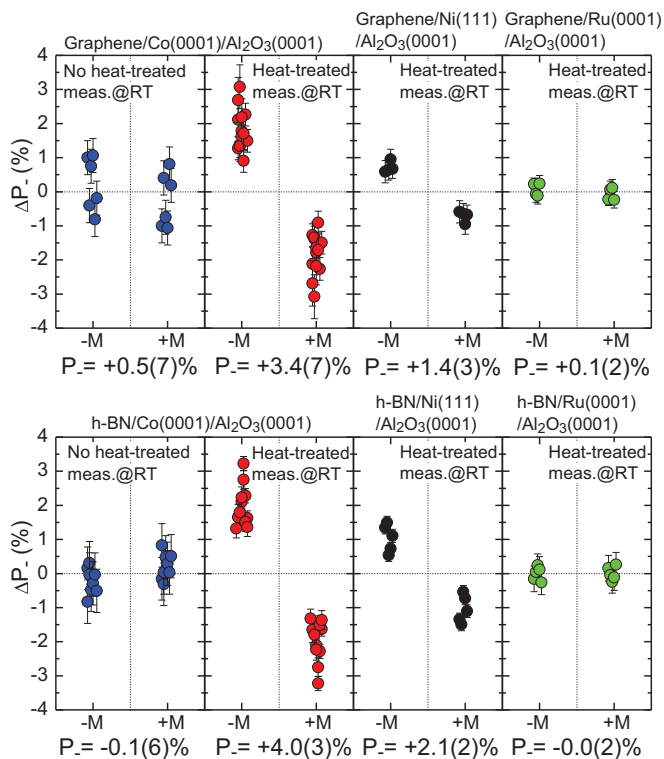


FIG. 2. Spin polarizations obtained for all the samples. The vertical axis is the shift of spin polarizations for positive (+ M) and negative ($-M$) magnetizations (see text). The net spin polarizations [$\Delta P_{-}(-M) - \Delta P_{-}(+M)$] are indicated below each panel.

The above results can be summarized as (i) the observed spin polarizations are induced from the ferromagnetic Co and Ni to graphene and *h*-BN, (ii) electrons detected as

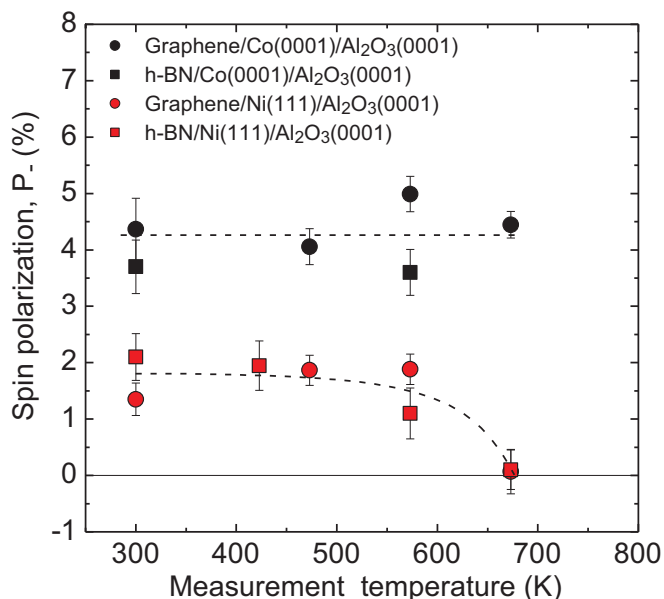


FIG. 3. Temperature dependence of spin polarizations obtained for graphene and *h*-BN on Co(0001) and Ni(111). The broken lines are guides for the eye.

positronium are positively spin polarized (majority spins are more abundant), (iii) the spin polarizations of graphene and *h*-BN on Co(0001) are higher than those on Ni(111), and (iv) the spin polarizations of graphene and *h*-BN are nearly the same on the same metal. From (i) we conclude that the magnetic proximity effect may exist. In (ii), the obtained signs of the spin polarization seem to be consistent with those in the SPMDS experiments [3,6]. Positrons may pick up electrons located not only at the Fermi level but also at deeper levels, i.e., from $E_F + \Phi_{Ps}$ to E_F , where Φ_{Ps} is the positronium work function (~ -3 eV for Co and Ni). Hence the spin polarization obtained by the present experiment is expected to be the average in this energy range. From (iii) and (iv) it is inferred that the electronic states of graphene and *h*-BN are strongly dominated by the metal characters. To confirm these speculations, we made the following first-principles calculations.

B. Theoretical calculations

After structural optimization, the interlayer distance between the graphene and Co(0001) or Ni(111) layer was 2.10 Å or 2.09 Å. The buckling between two inequivalent C atoms was 0.019 Å on Co(0001) and 0.007 Å on Ni(111). The interlayer distances between the *h*-BN and Co(0001) layers was 2.07 Å and that between the *h*-BN and Ni(111) layers was 2.06 Å. The buckling between B and N atoms was 0.12 Å on Co(0001) and 0.11 Å on Ni(111). N and B atoms are shifted outward and inward, respectively. These values are consistent with the previous report [22].

Figure 4 shows the electron density of states [denoted by DOS or $D(E)$] calculated through the ABINIT computation itself. For isolated graphene, the DOS profile reflects the Dirac cone at the K point. A band gap of 4.6 eV was obtained for isolated *h*-BN, although underestimation is a common problem in DFT calculations. In graphene on Co(0001) and Ni(111), the Dirac conelike DOS profile remains above the Fermi level, at least partially, but the profile below the Fermi level is strongly modulated due to d - π hybridization. As for *h*-BN on Co(0001) and Ni(111), the band gap completely disappears and the profile of the valence band is also significantly changed, again due to d - π hybridization. Thus *h*-BN attached to Co or Ni is expected to become metallic.

As mentioned above, when positronium is formed via the work function mechanism, positrons can capture electrons located from E_F to $E_F + \Phi_{Ps}$. Although the electron pick-up probability may be estimated in terms of the golden rule approach considering the wave functions of electrons, positrons, and positronium and also the effective Coulomb potential, we first assume that it is proportional to the density of states since the positronium time-of-flight (energy) spectrum may be approximated as the surface density of states [23]. In this case, the spin polarization would be given by

$$P_{-} = \frac{\int \{D^{\uparrow}(E) - D^{\downarrow}(E)\} dE}{\int \{D^{\uparrow}(E) + D^{\downarrow}(E)\} dE}, \quad (3)$$

where \uparrow (\downarrow) denotes the majority (minority) spin channel and the integration range may be from $E_F + \Phi_{Ps}$ up to E_F . However, the spin polarizations obtained using the DOS profiles shown in Fig. 4 did not give results that systematically

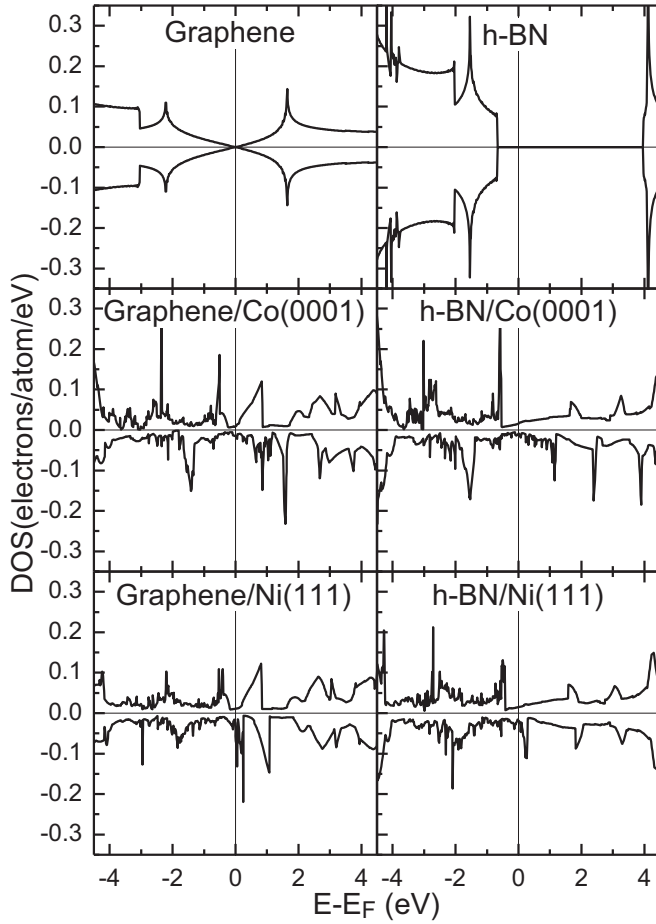


FIG. 4. Electron density of states (DOS) profiles calculated for graphene and *h*-BN in isolated form, on Co(0001) and on Ni(111).

explain the experimental data. The density of states of Fig. 4 is sampled only around atoms in spheres with typical diameters of 0.5 to 1 Å. For a better approximation, we calculated the electron-positron density of states (*e-p* DOS), which is defined here as the integration of the product of the electron

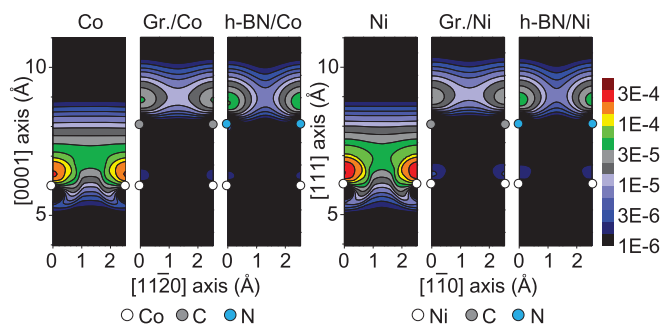


FIG. 5. Cross-sectional electron-positron density distributions calculated for Co, graphene/Co, and *h*-BN/Co on the (1100) plane and Ni, graphene/Ni, and *h*-BN/Ni on the (112) plane. The unit of the color bar is a_B^{-6} . White circles are Co and Ni atoms and gray and blue circles are C and N atoms, respectively. B atoms are not shown on these planes.

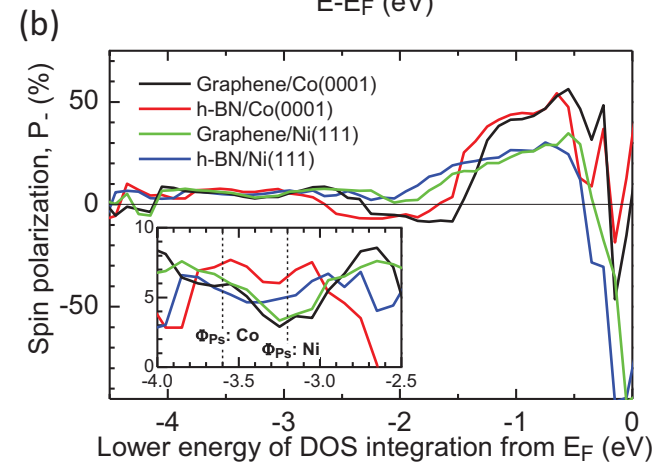
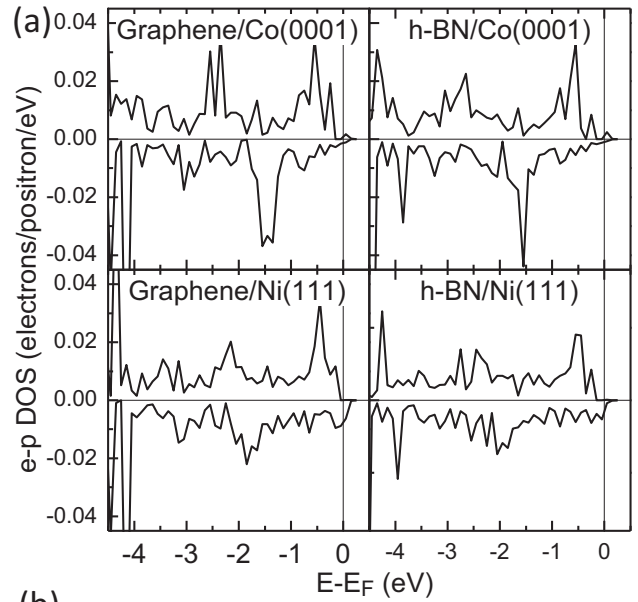


FIG. 6. (a) Electron-positron density of states (*e-p* DOS) calculated for graphene/Co(0001), *h*-BN/Co(0001), graphene/Ni(111), and *h*-BN/Ni(111). (b) Electron spin polarization calculated from Eq. (3) and the above electron-positron densities of states as a function of the lower energy of integration. The inset is a magnification of the region around the positronium work function.

density of states and the positron density at arbitrary positions in the total space, as follows.

The electron density of states at arbitrary positions was computed from the ABINIT outputs. In the calculation of positron density, any surface potentials and the enhancement factor based on the weighted density approximation [24] were not assumed, since in the work function mechanism positronium will be formed when positrons propagate in the vacuum side of the surface. That is, the positron state may be described as a plane wave or a scattering state in the surface potential, but not in the surface state, while the electron density decreases to less than $\sim 1/100$ from the first surface layer to ~ 2 Å vacuum side. Therefore, most simply, it may be enough to obtain the positron density which varies slowly but reflects the atomic configuration in such a thin layer. Here, we used the positron wave function in the vacuum region calculated using the updated parameter-free GGA enhancement factor [25].

Figure 5 shows the calculated electron-positron densities. (The positron density was renormalized to the integrated density in the region where the electron-positron density is above 1% of the maximum.) From this, electrons from the first surface layer to 1–2 Å vacuum side are sampled by positrons. This picture is basically the same as that expressed by the g function which was introduced for evaluating the matrix element and has a peak in the vacuum side of the surface [23]. From the viewpoint that positronium is not formed inside metals due to the screening of high density electrons, the present calculation may not give rise to serious problems. But, inner electrons will also be able to hop onto positrons in the vacuum region to form positronium when the Coulomb interaction acts effectively. If this process occurs with high enough probability, the present treatment underestimates the contribution from inner electrons. The evaluation of this process remains for the future. Nevertheless, the experimental spin polarizations are well reproduced, as shown below.

Figure 6(a) shows $e-p$ DOS profiles for graphene and *h*-BN on Co(0001) and Ni(111). Since positrons mainly exist in the vacuum region, the DOS profiles are reduced compared with the conventional DOS profiles shown in Fig. 4. Figure 6(b) shows the spin polarizations obtained using Eq. (3) and the DOS profiles of Fig. 6(a) as a function of the lower energy of integration from the Fermi level. Above -3 eV, the calculated spin polarization varies between positive and negative values and the magnitude is much greater than the experimental values. Hence, only considering such an energy region, the experimental data are hardly explained. In the present

calculations, $\Phi_{ps} = -3.6$ eV for Co and $\Phi_{ps} = -3.2$ eV for Ni. Spin polarizations at around these energies are $+6$ – $+7\%$ for graphene and *h*-BN on Co(0001) and $+4$ – $+5\%$ for graphene and *h*-BN on Ni(111). These values are only a few % larger than the experimental values in Fig. 2 and hence explain the experimental magnitude of the spin polarization. The other two experimental facts—that the spin polarizations of graphene and *h*-BN on Co(0001) are higher than those on Ni(111) and that the spin polarizations of graphene and *h*-BN on the same metals are comparable—are also explained by the above calculation.

V. SUMMARY

The spin polarizations for graphene and *h*-BN on Co(0001) and Ni(111) observed by spin-polarized surface positronium annihilation measurement were well explained by the present DFT calculation. Conversely, a series of features predicted in the calculation, such as the destruction of the Dirac cone of graphene and the disappearance of the band gap of *h*-BN due to hybridization with the metals, may be justified. Graphene and *h*-BN are spin polarized by contacting them to Co and Ni, but instead their original characteristics are lost significantly. If this is a problem when realizing graphene-based devices, some means to avoid it needs to be established.

ACKNOWLEDGMENT

This work was financially supported by JSPS KAKENHI under Grant No. 17K19061.

-
- [1] N. Tombros, C. Jozsa, M. Popinciuc, H. T. Jonkman, and B. J. van Wees, *Nature (London)* **448**, 571 (2007).
 - [2] T. Yamaguchi, Y. Inoue, S. Masubuchi, S. Morikawa, M. Onuki, K. Watanabe, T. Taniguchi, R. Moriya, and T. Machida, *Appl. Phys. Express* **6**, 073001 (2013).
 - [3] S. Entani, M. Kurahashi, X. Sun, and Y. Yamauchi, *Carbon* **61**, 134 (2013).
 - [4] P. Hota, A. J. Akhtar, S. Bhattacharya, M. Miah, and S. K. Saha, *Appl. Phys. Lett.* **111**, 042402 (2017).
 - [5] N. Rougemaille, A. T. N'Diaye, J. Coraux, C. Vo-Van, O. Fruchart, and A. K. Schmid, *Appl. Phys. Lett.* **101**, 142403 (2012).
 - [6] M. Ohtomo, Y. Yamauchi, A. A. Kuzubov, N. S. Eliseeva, P. V. Avramov, S. Entani, Y. Matsumoto, H. Naramoto, and S. Sakai, *Appl. Phys. Lett.* **104**, 051604 (2014).
 - [7] N. Joshi and P. Ghosh, *Phys. Rev. B* **87**, 235440 (2013).
 - [8] D. W. Gidley, A. R. Köymen, and T. W. Capelhart, *Phys. Rev. Lett.* **49**, 1779 (1982).
 - [9] A. Kawasuso, Y. Fukaya, M. Maekawa, H. Zhang, T. Seki, T. Yoshino, E. Saitoh, and K. Takanashi, *J. Magn. Magn. Mater.* **342**, 139 (2013).
 - [10] H. Zhang, Y. Fukaya, M. Maekawa, H. Li, A. Kawasuso, T. Seki, E. Saitoh, and K. Takanashi, *Sci. Rep.* **4**, 4844 (2014).
 - [11] H. Zhang, S. Yamamoto, B. Gu, H. Li, M. Maekawa, Y. Fukaya, and A. Kawasuso, *Phys. Rev. Lett.* **114**, 166602 (2015).
 - [12] S. Entani, Y. Matsumoto, M. Ohtomo, P. V. Avramov, H. Naramoto, and S. Sakai, *J. Appl. Phys.* **111**, 064324 (2012).
 - [13] Y. Matsumoto, S. Entani, A. Koide, M. Ohtomo, P. V. Avramov, H. Naramoto, K. Amemiya, T. Fujikawa, and S. Sakaia, *J. Mater. Chem. C* **1**, 5533 (2013).
 - [14] S. Marder, V. W. Hughes, C. S. Wu, and W. Bennett, *Phys. Rev.* **103**, 1258 (1956).
 - [15] K. G. Lynn and D. O. Welch, *Phys. Rev. B* **22**, 99 (1980).
 - [16] P. G. Coleman, *Solid State Phenom.* **28&29**, 179 (1992/93).
 - [17] R. M. Drisko, *Phys. Rev.* **102**, 1542 (1956).
 - [18] X. Gonze, J.-M. Beuken, R. Caracas, F. Detraux, M. Fuchs, G.-M. Rignanese, L. Sindic, M. Verstraete, G. Zerah, F. Jollet, M. Torrent, A. Roy, M. Mikami, P. Ghosez, J.-Y. Raty, and D. Allan, *Comput. Mater. Sci.* **25**, 478 (2002).
 - [19] P. E. Blöchl, *Phys. Rev. B* **50**, 17953 (1994).
 - [20] J. P. Perdew, K. Burke, and M. Ernzerhof, *Phys. Rev. Lett.* **77**, 3865 (1996).
 - [21] S. Grimme, *J. Comput. Chem.* **27**, 1787 (2006).
 - [22] P. Avramov, A. A. Kuzubov, S. Sakai, M. Ohtomo, S. Entani, Y. Matsumoto, H. Naramoto, and N. Eliseeva, *J. Appl. Phys.* **112**, 114303 (2012).
 - [23] A. P. Mills, L. Pfeiffer, and P. M. Platzman, *Phys. Rev. Lett.* **51**, 1085 (1983).
 - [24] A. Rubaszek, *Phys. Rev. B* **44**, 10857 (1991).
 - [25] B. Barbiellini and J. Kuriplach, *Phys. Rev. Lett.* **114**, 147401 (2015).